Relation between left ventricular cavity pressure and volume and systolic fiber stress and strain in the wall

Theo Arts,* Peter H. M. Bovendeerd,* Frits W. Prinzen,‡ and Robert S. Reneman‡
Departments of *Biophysics and ‡Physiology, University of Limburg, 6200MD Maastricht, The Netherlands

ABSTRACT Pumping power as delivered by the heart is generated by the cells in the myocardial wall. In the present model study global left-ventricular pump function as expressed in terms of cavity pressure and volume is related to local wall tissue function as expressed in terms of myocardial fiber stress and strain. On the basis of earlier studies in our laboratory, it may be concluded that in the normal left ventricle muscle fiber stress and strain are homogeneously distributed. So, fiber stress and strain may be approximated by single values, being valid for the whole wall. When assuming rotational symmetry and homogeneity of mechanical load in the wall, the dimensionless ratio of muscle fiber stress (σ_f) to left-ventricular pressure (P_{lv}) appears to depend mainly on the dimensionless ratio of cavity volume (V_{lv}) to wall volume (V_w) and is quite independent of other geometric parameters. A good ($\pm 10\%$) and simple approximation of this relation is $\sigma_f/P_{lv} = 1 + 3\,V_{lv}/V_w$. Natural fiber strain is defined by $e_f = \ln(l_f/l_{f,ref})$, where $l_{f,ref}$ indicates fiber length (l_f) in a reference situation. Using the principle of conservation of energy for a change in e_f, it holds $\Delta e_f = (1/3)\Delta \ln(1 + 3V_{lv}/V_w)$.

INTRODUCTION

The left venticle is an example of a cavity enclosed by a fibrous wall. The cavity can exchange mechanical power to the environment by changing volume at a certain cavity pressure. The work is generated or absorbed by the material in the wall. From a mechanical point of view the material in the wall may be considered as a soft, incompressible bulk material embedding a fibrous structure. Generally, most deformation energy is stored and exchanged by the fibrous structures formed by for instance collagen and muscle filaments. The soft nonfibrous bulk material cannot absorb or store large amounts of mechanical energy because it is incompressible, and easily deformable. So, absorption or delivery of mechanical power by the cavity is predominantly associated with absorption or generation of mechanical power by the fibers in the wall. The present study deals with a general relation between pressure in and volume of a cavity and mechanical load of the fibers in the wall.

In the in vivo situation direct measurement of muscle fiber stress is difficult. Transducers inserted into the wall (Feigl et al., 1967; Huisman et al., 1980) to measure stress, damage the tissue at the site of measurement. Direct measurement of stress may be circumvented by introduction of mathematical models of the mechanics of the chamber wall. A review of such models has been presented by Yin (1981). The early, simple models assume a thin-walled chamber obeying Laplace's law (Woods, 1892). In a newer generation of models, the left ventricle is considered to be thick-walled, having isotropic material properties. At this point, several investigators calculated the ratio of mid-wall stress to left-ventricular pressure on the basis of a thick-walled spherical (Mirsky, 1973) or ellipsoidal (Mirsky, 1969; Falsetti, 1970; Kim, 1985) geometry. A more accurate description of the geometry of the heart required the use of the finite-element calculation technique, applied to an ellipsoidal (Janz, 1982) or more realistic geometry with isotropic (Pao et al., 1976) or anisotropic (Perl et al., 1986; Huyghe, 1986) material. The results obtained with the models using isotropy were essentially similar as far as the transmural distribution of stress is concerned, regardless of the complexity of their geometry. In these models, both stress and strain were often more than twice as high in the subendocardial than in the subepicardial layers. In models the transmural gradient in stress can be reduced easily by introducing an artificial prestress and strain in the reference state. But even then changes in stress during deformation showed essentially unaltered transmural differences.

When introducing anisotropic properties in the thick wall, the transmural course of fiber stress appeared to be qualitatively and quantitatively different (Arts et al., 1979; Beyar et al., 1984; Chadwick, 1982). With a proper choice of the transmural course of fiber orientation close to anatomical findings (Streeter and Hanna, 1973), and introduction of torsional deformation, fiber stress was calculated to be homogeneous with $< \pm 10\%$ deviation

Dr. Arts' current address is Department of Biophysics, University of Limburg, PO Box 616, 6200MD Maastricht, The Netherlands.

0006-3495/91/01/93/10 $2.00

from the average stress (Arts et al., 1982) under a wide variety of loading conditions. Such homogeneity in mechanical load is supported by an experimental study (Waldman et al., 1988) in which transmural differences in strain along the fiber direction were found to be below the level of significance. When postulating homogeneity of fiber stress and fiber strain in the thick wall enclosing a cavity, significant simplications can be introduced (Regen, 1984, 1988; Skalak, 1982; Arts and Reneman, 1987, 1988). Regen showed that average fiber stress could be estimated on the basis of left-ventricular pressure and wall dimensions without solving the transmural distribution of fiber stress in detail. He also mentioned that the ratio of cavity volume to wall volume was a major determinant of the ratio of fiber stress to left-ventricular pressure. Skalak showed that left-ventricular pressure can be calculated by integration of the regional product of fiber stress and fiber curvature along a path from the epicardium to the endocardium. However, on the basis of the latter equation, left-ventricular pressure cannot be related to fiber stress directly, because radius of fiber curvature is determined by the unknown local geometry and fiber orientation.

In the present study we have investigated how accurately left-ventricular pressure and volume can be related to fiber stress and fiber strain, when using only one single geometric parameter, namely the ratio of cavity volume to wall volume. We postulate homogeneity of fiber stress and fiber strain in the thick wall enclosing a cavity. The stress in the incompressible, soft, nonfibrous bulk material of the wall is described by a hydrostatic pressure, implying a fluidlike behavior of the bulk material between the fibers. Under these assumptions, for a rotationally-symmetric geometry, cavity pressure is expressed in terms of fiber stress, cavity volume, wall volume, and cavity shape. In a second step, based on the principle of conservation of energy, fiber strain is calculated as a function of cavity volume. Thus, the calculated results may describe mechanical properties of the left-ventricular chamber, and other biological chambers with a fibrous wall like the bladder, the uterus as well as blood vessels.

FIBER STRESS IN A THIN-WALLED ROTATIONALLY-SYMMETRIC CHAMBER

In the present study, myocardial material is considered to be a soft incompressible material, embedding muscle fibers. During systole, when fiber stress is high, in the soft bulk of the tissue hydrostatic pressure (P_{im}) is the only stress component. For the stress along (σ_1) and perpendicular to (σ_2) the fiber direction it holds,

$$\sigma_1 = -P_{im} + \sigma_f \tag{1}$$

$$\sigma_2 = -P_{im}, \tag{2}$$

where σ_f represents the tensile stress in the fibers.

In a thin-walled geometry, the fibers are directed parallel to the surface. Assuming that β represents the angle between the fibers and circumference at the c-coordinate in the surface (Fig. 1), for the components of fiber stress along the circumference σ_{cc}, along the perpendicular t coordinate σ_{tt}, and perpendicular to the surface σ_{hh} it holds (Arts et al., 1979):

$$\sigma_{cc} = -P_{im} + \sigma_f \cos^2 \beta \tag{3}$$

$$\sigma_{tt} = -P_{im} + \sigma_f \sin^2 \beta \tag{4}$$

$$\sigma_{hh} = -P_{im}. \tag{5}$$

From these equations fiber stress σ_f can be found by:

$$\sigma_f = \sigma_{cc} + \sigma_{tt} - 2\sigma_{hh}. \tag{6}$$

Eq. 6 is an interesting and important result, and shows that fiber stress can be expressed in terms of perpendicular components of stress, irrespective of the actual fiber orientation in the ct-plane.

Fig. 2 represents a thin-walled rotationally-symmetric shell with r, c, and z being the radial, circumferential and axial coordinates, respectively. The surface is described by the function $r(z)$. In a point S at the surface, the t

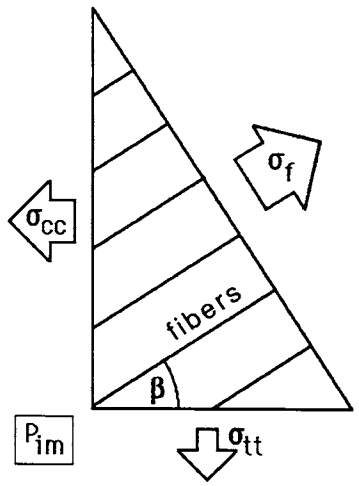

FIGURE 1 Fiber stress σ_f equals the sum of perpendicular fiber stress components. The fiber stress components may be obtained from the perpendicular stress components σ_{cc} and σ_{tt} after subtraction of the hydrostatic pressure P_{im} in the soft, incompressible material surrounding the fibers.

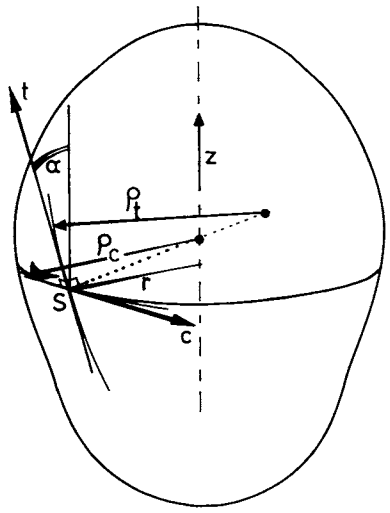

FIGURE 2 Thin-walled rotationally-symmetric shell. The variables r and z are the radial and axial coordinate, c and t are the circumferential and tangential coordinate in point S on the shell, ρ_c and ρ_t refer to circumferential and tangential radius of curvature.

coordinate is the tangent of the surface perpendicular to the c direction. For the calculation of fiber stress in the thin wall in point S we define the angle α as the angle between z and t direction, and ρ_c and ρ_t as the radii of curvature of the surface along the c and t direction, respectively.

Assume a pressure difference, ΔP, across the thin wall, while the average of cavity pressure and outer pressure is zero. Then the stress component σ_{hh} may be neglected. The stress component σ_{tt} along the t direction causes a total axial force component F_z on the edge of the cross-sectional circle through S:

$$F_z = 2\pi r h \sigma_{tt} \cos\alpha, \tag{7}$$

where h represents wall thickness. This force is equal to the force exerted by the pressure difference ΔP across the wall acting on the circular area of the cross-section ($F_z = \Delta P \pi r^2$). Elimination of F_z results in

$$\sigma_{tt} = \frac{\Delta P r}{2h \cos\alpha}. \tag{8}$$

As now will be shown, wall thickness h may be expressed as a function of z. According to Laplace's law for a thin-walled membrane it holds

$$\Delta P = \frac{\sigma_{tt} h}{\rho_t} + \frac{\sigma_{cc} h}{\rho_c}. \tag{9}$$

The angle α and the radii of curvature depend on the function $r(z)$ by

$$\cos\alpha = \left[1 + \left(\frac{dr}{dz}\right)^2\right]^{-1/2} \tag{10}$$

$$\rho_t = -\left(\frac{d^2r}{dz^2}\cos^3\alpha\right)^{-1} \tag{11}$$

$$\rho_c = \frac{r}{\cos\alpha}. \tag{12}$$

The stress component σ_{cc} in Eq. 9 may be eliminated using Eq. 6 and $\sigma_{hh} = 0$. Next, the component σ_{tt} is eliminated by using Eq. 8. With Eqs. 10–12, the radii of curvature ρ_t and ρ_c as well as $\cos\alpha$ are eliminated. So, finally wall thickness may be expressed as a function of pressure P, fiber stress σ_f, and the geometric function $r(z)$ by

$$h = \frac{\Delta P r}{2\sigma_f}\left[3 + 3\left(\frac{dr}{dz}\right)^2 + r\frac{d^2r}{dz^2}\right]\cdot\left[1 + \left(\frac{dr}{dz}\right)^2\right]^{-1/2}. \tag{13}$$

Using our hypothesis that fiber stress σ_f is homogeneously distributed, the volume V_{sh} of the thin-walled shell is found by integration of the cross-sectional area of the wall over the axial length of the rotationally-symmetric geometry. Using Eq. 13 it holds

$$V_{sh} = \int_{z_{min}}^{z_{max}} \frac{2\pi r h}{\cos\alpha} dz = \int_{z_{min}}^{z_{max}} \frac{\Delta P \pi r^2}{\sigma_f}\left[3 + 3\left(\frac{dr}{dz}\right)^2 + r\frac{d^2r}{dz^2}\right] dz. \tag{14}$$

The boundaries z_{min} and z_{max} indicate the axial dimension of the shell. The integral Eq. 14 can be split and rewritten as

$$V_{sh} = \frac{3\Delta P}{\sigma_f}\int_{z_{min}}^{z_{max}} \pi r^2\, dz + \frac{\pi\Delta P}{\sigma_f}\int_{z_{min}}^{z_{max}}\left[3r^2\left(\frac{dr}{dz}\right)^2 + r^3\frac{d^2r}{dz^2}\right] dz$$

$$V_{sh} = \frac{3\Delta P V}{\sigma_f} + \frac{\pi\Delta P}{4\sigma_f}\int_{z_{min}}^{z_{max}} \frac{d^2(r^4)}{dz^2} dz, \tag{15}$$

where V equals the inner volume enclosed by the shell. The integral of the second derivative is equal to the first derivative, so it follows

$$V_{sh} = \frac{3\Delta P V}{\sigma_f} + \frac{\pi\Delta P}{4\sigma_f}\cdot\left\{\left[\frac{d(r^4)}{dz}\right]z = z_{max} - \left[\frac{d(r^4)}{dz}\right]z = z_{min}\right\}$$

$$= \frac{3\Delta P(V + V_{err})}{\sigma_f}. \tag{16}$$

The volume V_{err} expresses the error volume introduced by the last integral term. Physically, the error volume equals the volume of the cone with the top at the

intersection of the axis of symmetry and the line perpendicular to the surface, and with the base being the cut-off cross-section. V_{err} is equal to zero, if for $z = z_{max}$ and $z = z_{min}$ the derivative $dr^4/dz = 0$. This is the case if the cavity is closed with finite radius of curvature at the axis, or open with $dr/dz = 0$. The condition of finite radius of curvature is even more stringent than strictly needed.

Thus, a general result is found, being valid for all thin-walled ($V_{sh} \ll V$) rotationally-symmetric geometries, which are closed or open with $dr/dz = 0$ at the end. The sphere, ellipsoid as well as the cylinder are just special cases of this large family. It holds

$$\frac{\Delta P}{\sigma_f} = \frac{V_{sh}}{3V}. \tag{17}$$

Early in the derivation it is assumed that the average of inner and outer pressure equals zero so that σ_{hh} and P_{im} in Eqs. 1 and 5 are zero too. When adding a hydrostatic pressure P to both inner and outer pressure, σ_{hh} and P_{im} both increase with P, but the result of Eq. 17 remains unaffected. This is because hydrostatic pressure cannot store deformation energy in incompressible structures.

The most important implication of Eq. 17 is the fact that the dimensionless ratio of transmural pressure to fiber stress depends solely on the dimensionless ratio of shell volume to cavity volume, whereas the actual shape of the shell is irrelevant, as long as it is rotationally symmetric.

FIBER STRESS IN A THICK-WALLED ROTATIONALLY-SYMMETRIC CHAMBER

The relation between fiber stress σ_f and left-ventricular cavity pressure (P_{lv}) in a thick-walled rotationally-symmetric geometry is found by integration of pressure increments over a sufficient number of thin fitting shells. It is assumed that fiber stress is homogeneous in the thick wall and that the fibers are directed parallel to the isobaric surfaces. Using the result of Eq. 17 inside the wall, for the derivative of the hydrostatic pressure P_{im} with respect to enclosed volume V it holds within the wall

$$\frac{dP_{im}}{dV} = \frac{-\sigma_f}{3V}. \tag{18}$$

The negative sign is introduced because the pressure gradient is negative towards the outer wall. Integration of Eq. 18 from the outer wall surface ($V = V_{lv} + V_w$), where pressure is assumed to be zero, to the inner wall surface ($V = V_{lv}$) results in

$$\frac{P_{lv}}{\sigma_f} = \frac{1}{3} \ln\left(1 + \frac{V_w}{V_{lv}}\right), \tag{19}$$

with V_{lv} and V_w being cavity and wall volume, respectively. For a ratio V_w/V_{lv} much smaller than unity, Eq. 19 simplifies to Eq. 17. Eq. 19 implies that, when assuming rotational symmetry, the isobaric surfaces being parallel to the fibers, and fiber stress being homogeneous, the dimensionless ratio of cavity pressure to fiber stress depends solely on the dimensionless ratio of cavity volume to wall volume, and appears to be independent of other geometric factors. Eq. 19 has been derived earlier by Regen (1984) for the special case of an ellipsoid at the equator.

In Figs. 3 and 4 fiber stress relative to left-ventricular pressure (σ_f/P_{lv}) is plotted as a function of left-ventricular volume relative to wall volume (V_{lv}/V_w) for various models. Typically relative volume is in the range from 0.15–0.70, which is indicated by a horizontal, shaded bar. In Fig. 3 the line marked with *ln* represents the results obtained with Eq. 19. The thin lines (*cyl*) are obtained from simulations by a cylindric model of the fibrous left ventricle including mitral valve and right-ventricular asymmetry of fiber orientation (Arts and Reneman, 1989). Fiber stress as shown has been averaged over wall volume. Systoles of five beats with different preloads and afterloads are analyzed. The relation appears to be nearly perfectly linear, and the different beats closely coincide. The line *lin* represents a simple linear approximation to this model (Arts et al.,

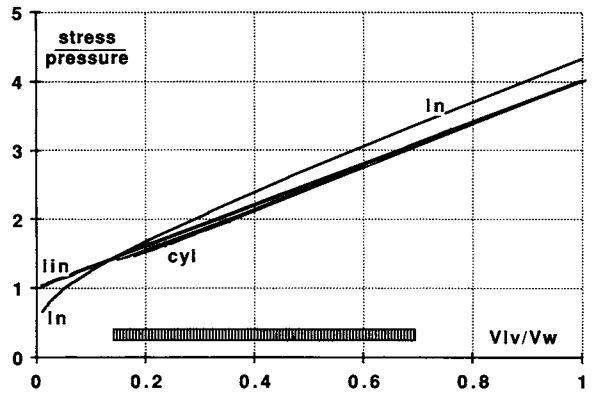

FIGURE 3 Calculated fiber stress relative to left-ventricular pressure as a function of cavity volume relative to wall volume. The shaded bar indicates the physiological range of the latter variable. Different curves refer to different models *ln*: Eq. 19 in this article; *cyl*: cylinder (Arts and Reneman, 1989); *lin*: linear approximation of *cyl* (Eq. 20).

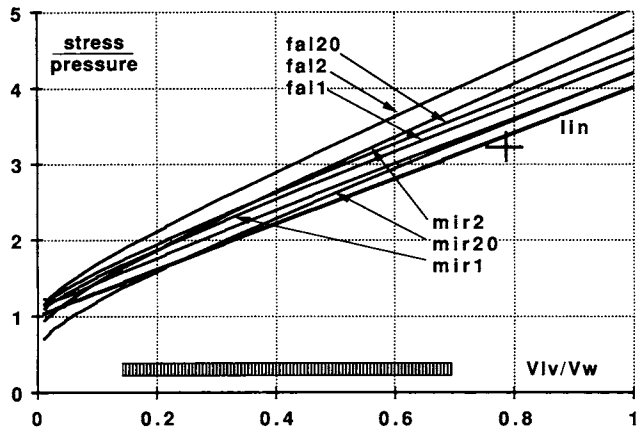

FIGURE 4 Calculated relative effective fiber stress using Eq. 6, plotted as a function of relative cavity volume. The curves *fal 1*, *fal 2*, and *fal 20* refer to the model of thick-walled ellipsoids (Falsetti et al., 1979; Kim et al., 1985) with axis ratio of 1:1, 1:2, and 1:20, respectively. Similarly, *mir 1*, *mir 2*, and *mir 20* refer to the model by Mirsky (1973). The cross-mark indicates the cylindric model of Chadwick (1982). The curve *lin* has been added for comparison with Fig. 3.

1982), expressed by

$$\frac{\sigma_f}{P_{lv}} = 1 + 3\frac{V_{lv}}{V_w}. \tag{20}$$

In Fig. 4 fiber stress is calculated by applying Eqs. 5 and 6 to the midwall stress components as found at the equator on the basis of models using isotropic material properties, and as presented by Mirsky (1973), Kim et al. (1985), and Falsetti et al. (1970). The latter two models are essentially the same. For comparison with Fig. 3, the results obtained by the linear approximation of Eq. 20 are duplicated. The cross-mark indicates a result obtained by the model of Chadwick (1982), applying a cylindric, anisotropic myocardial wall. Calculated effective fiber stress appears to depend on the ellipticity, having the values 1:1 (sphere), 1:2, and 1:20. Generally, spherical geometry is closest to Eq. 19. Ellipticity 1:2 shows the highest values of relative fiber stress.

Despite the wide variation in model setups used, all equations shown in Figs. 3 and 4 are similar. Relative fiber stress increases with relative cavity volume, which agrees with the fact that stress increases with increasing radius of curvature and decreasing wall thickness. Fiber stress appears to be determined mainly by cavity pressure and the ratio of cavity volume to wall volume and is quite unaffected by the actual choice of material properties, geometric factors or the inhomogeneity of stress distribution across the wall. In case of isotropic wall material, an effective fiber stress is calculated, having properties similar to real fiber stress in models based on anisotropy.

FIBER STRAIN

It is assumed that the principle of conservation of energy may be applied, i.e., mechanical work is generated by the myocardial fibers in the entire wall is equal to pumping work of the left-ventricular chamber. Then it holds

$$\int_{V_w} \sigma_f \Delta e_f \, dV = P_{lv} \Delta V_{lv}, \tag{21}$$

where e_f represents natural fiber strain (ln $[l/l_{ref}]$), and Δ is associated with a small increment in left-ventricular cavity volume. Using the assumption that fiber stress and strain are homogeneously distributed, Eq. 21 may be converted to the following differential form

$$\frac{de_f}{d\frac{V_{lv}}{V_w}} = \frac{P_{lv}}{\sigma_f}. \tag{22}$$

Figs. 5 and 6 show natural fiber strain, as calculated by integration of Eq. 22 with respect to relative cavity volume, and as applied to the relations shown in Figs. 3 and 4. The reference length of strain is chosen so that $e_f = 0$ at $V_{lv} = 0$. A change in natural fiber strain Δe_f during ejection may be obtained by subtraction of the values of e_f, as calculated for begin and end of ejection, respectively. In Fig. 5 the line *ln* is obtained by integration of Eq. 19 with respect to V_{lv}/V_w:

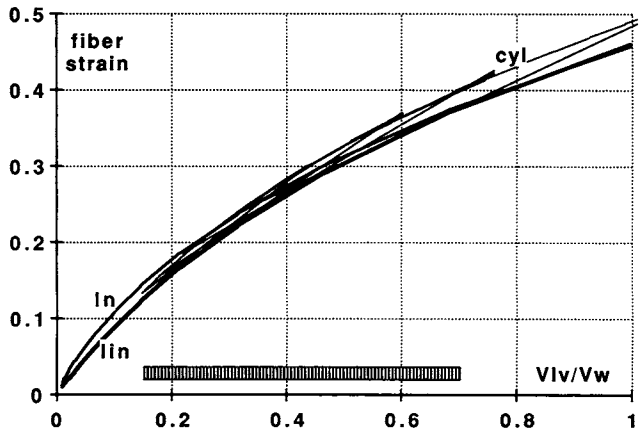

FIGURE 5 Calculated natural fiber strain (ln $[l/l_{ref}]$) as a function of relative cavity volume. For identification of the curves, see legends Fig. 3. Fiber strain is defined to be zero in the reference situation at zero cavity volume.

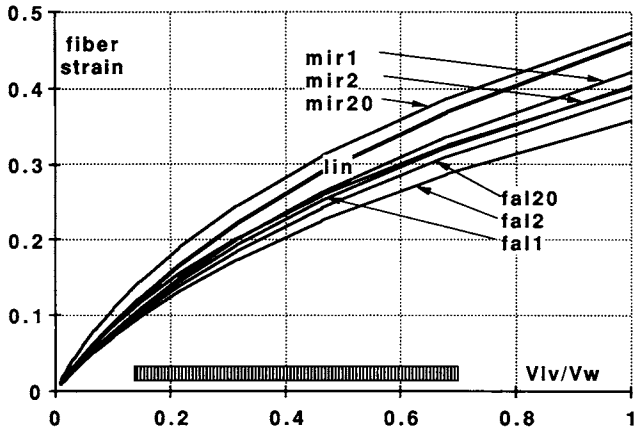

FIGURE 6 Calculated natural fiber strain as a function of relative cavity volume. For identification of the curves, see legends Fig. 4.

$$e_f = \int_{V_{lv}=0}^{V_{lv}} \frac{1}{3} \ln\left(1 + \frac{V_w}{V_{lv}}\right) d\frac{V_{lv}}{V_w}$$
$$= \frac{1}{3}\left(\left(1 + \frac{V_{lv}}{V_w}\right) \ln\left(1 + \frac{V_{lv}}{V_w}\right) - \frac{V_{lv}}{V_w} \ln\left(\frac{V_{lv}}{V_w}\right)\right). \quad (23)$$

The line *lin* refers to the linear relation between relative fiber stress and volume according to Eq. 20. The related equation for fiber strain e_f is obtained by:

$$e_f = \int_{V_{lv}=0}^{V_{lv}} \left(1 + 3\frac{V_{lv}}{V_w}\right)^{-1} d\frac{V_{lv}}{V_w} = \frac{1}{3} \ln\left(1 + 3\frac{V_{lv}}{V_w}\right). \quad (24)$$

For the five beats in the cylinder model, fiber strain has been averaged over wall volume, and plotted as a function of relative left-ventricular volume. These curves are also shown in Fig. 5. In Fig. 6 fiber strain is obtained by numerical integration of the reciprocate of relative stress with respect to relative cavity volume (Eq. 22) for the models presented by Falsetti et al. and Mirsky. From the Figs. 5 and 6 the relation between fiber strain and relative cavity volume appears to be moderately dependent on the choice of the model.

The relation between fiber strain and ventricular pressure has not been theoretically evaluated as extensively as the relation between stress and left-ventricular pressure. After all, in a majority of models using isotropic properties of the wall material, fiber strain cannot be easily interpreted. A more understandable description of the relation between fiber strain and cavity volume may be given by the fraction of wall volume which has to be added to cavity volume in order to obtain a strain in that layer of the wall, which is equal to fiber strain. Mathematically, this wall fraction V_i/V_w has been obtained by solving the equation:

$$\Delta e_f = \frac{1}{3} \Delta \ln\left(\frac{V_{lv} + V_i}{V_w}\right). \quad (25)$$

The fraction V_i/V_w is expected to be in the range between 0 and 1, because fiber strain is likely to be smaller than strain at the inner surface ($V_i/V_w = 0$) and larger than this strain at the outer surface ($V_i/V_w = 1$). Using the data obtained in relation to Figs. 5 and 6, the volume V_i has been calculated by taking the derivative of Eq. 25 with respect to V_{lv} and reordering, which results in:

$$\frac{V_i}{V_w} = \frac{1}{3} \frac{d\frac{V_{lv}}{V_w}}{de_f} - \frac{V_{lv}}{V_w}. \quad (26)$$

In Figs. 7 and 8 the value of V_i/V_w, thus calculated, has been plotted as a function of relative volume. In Fig. 7, the lines *ln* and *lin* refer to the models associated with Eqs. 19 and 20, respectively. For the five beats in the cylinder model the derivative of fiber strain with respect to relative left-ventricular volume, as needed in Eq. 26 is determined as the slope of a quadratic curve fit to the relation between fiber strain and relative cavity volume. In Fig. 7 the related data points are indicated by the line *cyl*. In Fig. 8, the value of V_i/V_w is calculated on the basis of the models of Falsetti et al. and Mirsky. In all models, except for the model presented by Falsetti et al., the value of V_i/V_w is in the range between 0.2 and 0.45 for the regular range of relative volume, being from 0.15–0.70. In the model with linear stress-volume relation according to Eq. 21 the value of V_i/V_w is constant and equal to ⅓.

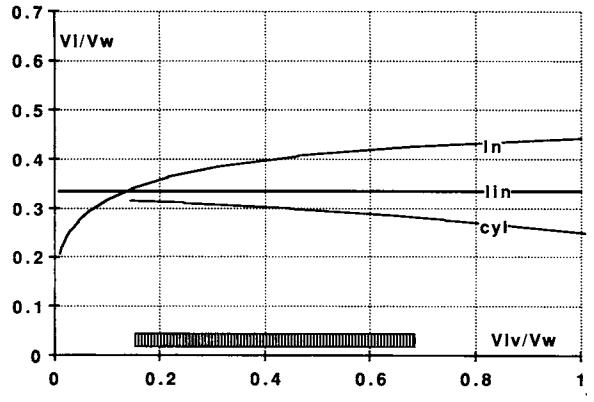

FIGURE 7 The fraction (V_i/V_w) of the wall that should be added to cavity volume is calculated so that strain in that layer of the wall is similar to fiber strain. This fraction is plotted as a function of relative cavity volume (V_{lv}/V_w). For identification of the curves, see legends Fig. 3.

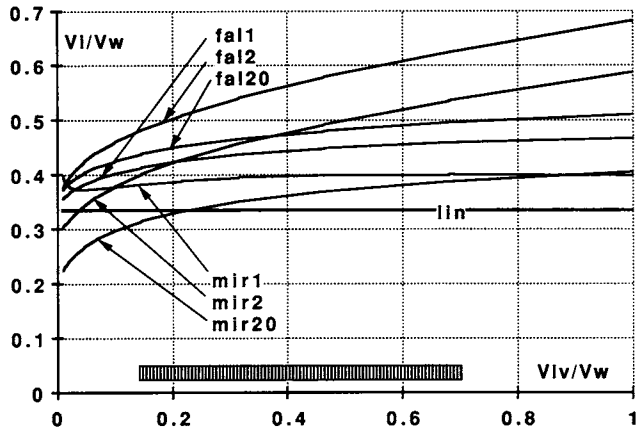

FIGURE 8 Wall fraction as defined in the legends of Fig. 7 as a function of relative cavity volume. For identification of the curves, see legends Fig. 4.

ERROR ESTIMATES

In the model *ln*, the accuracy of Eq. 17 is essential to the derivation of the equations for fiber stress (Eq. 19) and fiber strain (Eq. 23). The error in this equation is expressed by error term V_{err} in Eq. 16. As mentioned, this term equals zero if the volume is closed, or $dr/dz = 0$ at the boundary. In the real left ventricle at the basal boundary, none of these conditions are satisfied. Therefore, in a few examples we have calculated the maximum error to be expected from cutting off a cavity. Let us consider a thin-walled prolate ellipsoid with minor axis $2R$, and a major to minor axis ratio of a. The center is placed in the origin, and the ellipsoid is cut off at $z = z_{max}$. Then for the volume V within the cavity and the error volume term V_{err}, it holds

$$V = \frac{\pi a R^3}{3}(2 + 3Z - Z^3)$$

$$V_{err} = \frac{\pi R^3}{3a}(Z - Z^3)$$

$$\text{with } Z = \frac{z_{max}}{aR}. \qquad (27)$$

By differentiation of the ratio V_{err}/V with respect to z_{max}, at positive z_{max} the maximum error is found to occur at $z_{max} = 0.5\,aR$. Thus, using Eq. 16, for a sphere ($a = 1$) the overestimation of fiber stress is maximally 11%. The real left ventricle resembles a prolate ellipsoid with a long to short axis ratio of two or more ($a \geq 2$). Then the error in Eq. 16 is found to be <3%, which may be neglected under most circumstances.

A second source of error cannot be assessed quantitatively as easily. In the derivation of Eq. 16 the shell is considered to be in internal equilibrium, without being subject to external forces other than hydrostatic pressure. Moreover, the fibers are assumed to be parallel to the isobaric surfaces in the wall. So, strictly considered, for the heart the integral needed for Eq. 19 may not be used, because a number of muscular fibers mutually connect the different shells. In the real heart muscle fibers in the inner layers of the wall continue their course in the outer layers passing through the apex or bending over the rim of the base (Puff, 1960; Torrent Guasp, 1971). Considering the comparison of the results with different models as presented in Figs. 3 and 4, the errors thus introduced may be moderate.

DISCUSSION

In the present study equations are derived relating fiber stress, fiber strain, left-ventricular pressure, and left-ventricular volume. In the derivation which relates the ratio of fiber stress and left-ventricular pressure to the ratio of cavity to wall volume, it is assumed that the myocardial material is soft and incompressible, embedding stress bearing muscle fibers. During diastole muscle fibers are not activated implying that stresses in the passive, soft material cannot be neglected. During systole the muscle fibers are activated and bear stress far above the passive stress level associated with diastole. So during systole anisotropy of the kind as assumed is probably far more pronounced than during diastole. Hence, the presented equations on fiber stress and strain are expected to be a more accurate description of the systolic phase rather than of the diastolic phase of the cardiac cycle.

In Fig. 3 the ellipsoidal models described by Falsetti et al. (1970) and Kim et al. (1985) show somewhat higher values for fiber stress than the other models. In these models, apical and equatorial wall thickness are considered to be the same. Because the radii of curvature at the equator are larger than at the long axis poles, in these models stress in the wall at the poles is lower than at the equator. Hence, equatorial stress as shown is an overestimation of mean stress. This discrepancy vanishes for a spherical as well as a cylindrical geometry. For a minor to major axis ratio of 1:2 this effect is nearly maximal.

In many studies, the circumferential component of wall stress is described and discussed as if it were a

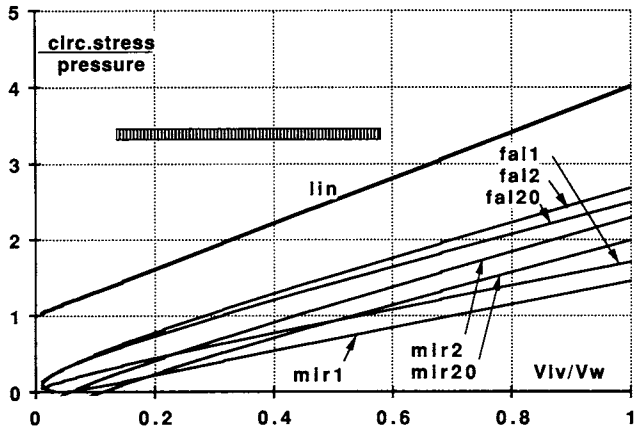

FIGURE 9 Calculated ratio of the circumferential stress relative to left-ventricular pressure, as a function of relative cavity volume. For identification of the curves, see legends Fig. 4.

representative for fiber stress. In Fig. 9, relative circumferential stress as calculated with the models presented by Falsetti et al. and Mirsky are shown as a function of relative cavity volume. For comparison, the linear relation *lin* for fiber stress is also shown. As may be expected on the basis of Eq. 6, circumferential stress is smaller than fiber stress. Moreover, this stress component is sensitive to the actual shape of the left ventricle. When neglecting intramyocardial pressure, for a sphere this stress is 50% of fiber stress, and for a cylinder 67%. For extremely low volumes, circumferentially directed stress approaches zero. This paradoxical result is associated with the fact that hydrostatic intramyocardial pressure in the bulk compensates for the circumferential stress component born by the fibers. Because fiber stress is not as sensitive to shape as circumferential stress, this stress is preferred in relating pumping work to myocardial fiber work.

Left-ventricular pressure has been obtained by integration of pressure increments from the outer to the inner shell. Similarly, Skalak (1982) has proposed to calculate left-ventricular pressure by integration of pressure increments associated with the regional radius of fiber curvature. Both methods require that the fibers are perpendicular to the direction of the pressure gradient. In our derivation this means that the fibers do not leave the shell defined as to be enclosed between two isobaric surfaces. In the equatorial region this assumption might be realistic, but in the apical and basal regions muscle fibers in the subendocardial layers continue in the subepicardium (Torrent Guasp, 1971; Streeter et al., 1973; Puff, 1960). So, fibers cross isobaric surfaces. As a result, part of the fiber contraction work is transferred from the subepicardium to the subendocardium along the fibers by shear stress along isobaric surfaces, and not only by the mechanism associated with building up of hydrostatic pressure from the epicardium towards the endocardium. Macroscopically, the energy transfer along the fibers is associated with torsion of the left ventricle, which is thought to be a mechanism of transmural redistribution of fiber strain (Arts et al., 1979; Arts and Reneman, 1989).

In the derivation relating relative fiber stress to relative cavity volume, the shape of the shells is assumed to be invariant. Generally, systems of nonspherical shells have to change shape during large deformations as long as the shells have a constant volume and fit without interspacings. In the real left ventricle and the cylindric model (Arts and Reneman, 1989), the inner shells shorten much more circumferentially than axially. This shape change has consequences for the stress–volume relationship. The average change of fiber strain Δe_f depends on a small change in relative cavity volume V_{lv}/V_w and shape factor s by:

$$\Delta e_f = \frac{\partial e_f}{\partial \frac{V_{lv}}{V_w}} \Delta \frac{V_{lv}}{V_w} + \frac{\partial e_f}{\partial s} \cdot \Delta s + \frac{1}{2} \frac{\partial^2 e_f}{\partial s^2} \cdot (\Delta s)^2. \qquad (28)$$

Because no external forces are loading the ventricle, shape varies until potential energy is minimal. It is assumed that fiber stress is homogeneously distributed, so s varies until fiber length is minimal. Hence, around the state of equilibrium, the first derivative of fiber length with respect to the shape factor s is equal to zero. Furthermore, because strain is minimum, $\partial^2 e_f/\partial s^2$ is positive.

So, the value of Δe_f is always more positive than as to be expected when there was no shape constraint to volume. The principal of conservation of energy (Eq. 22) may be written as

$$\frac{\sigma_f}{P_{lv}} = \frac{\Delta(V_{lv}/V_w)}{\Delta e_f}. \qquad (29)$$

When ΔV_{lv} and Δe_f both are positive, relative stress will increase less than in absence of a shape constraint due to an extra elevation of Δe_f. Similarly, for negative ΔV_{lv} and Δe_f, relative stress will decrease less than without shape constraint. As a result, the slope of relative stress versus relative volume decreases due to shape restraints as long as the principle of conservation of energy is satisfied. In Fig. 3 this behavior is found indeed when comparing the stress–volume curve of the shape-restrained cylinder with the model *ln*, which is associated with Eq. 19.

Using different models, the relation between relative fiber stress and volume are quite similar. In absence of

forced shape changes due to geometric constraints during deformation, the relation between relative stress and relative volume is independent of the shape of the cavity. When introducing effects of shape constraints, the slope of the curve decreases, and the curve may depend on geometry. In a cylinder model, empirically a linear relation between relative stress and relative volume is found. A good and simple approximation of this relation is $\sigma_f/P_{lv} = 1 + 3\,V_{lv}/V_w$. When using other models with spherical, ellipsoidal or cylindrical geometry, the fiber stress–volume relation is comparable to the latter approximation (Fig. 4). This indicates that the influence of geometric restraints is present, but moderate in character.

Using the principle of conservation of energy, the relation between relative fiber stress and volume may be transformed to a relation between fiber strain and cavity volume. Because in the various models stresses are found to be similar, the dependency of strain on volume is also quite similar for the various models. As indicated by Figs. 7 and 8, in the regular range of relative cavity volume ($0.15 \leq V_{lv}/V_w \leq 0.7$), strain can be approximated as the relative change in diameter of a sphere containing cavity volume and ⅓ of the wall volume.

In the cylinder model, fiber strain has been calculated directly, thus circumventing the assumption of muscle fiber work being equal to pumping work. Fiber strains, thus found, are similar to the strains as found using the stress–volume relation. The moderate difference between both strain curves may be explained by violation of the assumption on homogeneity of fiber stress, or the fact that pumping work may not be equal to the work in the myocardial wall considered. After all, the effect of right-ventricular stresses on the left-ventricular deformation has been partly included in the cylinder model causing an energetic cross-talk between left- and right-ventricular walls. Moreover, stress in the nonmuscular leaflets of the mitral valve may have an effect too.

CONCLUSION

In a fibrous shell model it is assumed that the left-ventricular wall is rotationally symmetric, and consists of a fiber structure embedded in a soft incompressible material. Fiber stress is homogeneous. As a result it is found that the ratio of fiber stress (σ_f) to left-ventricular pressure (P_{lv}) depends mainly on the ratio of cavity volume (V_{lv}) to wall volume (V_w). The shape of the cavity appears of minor importance. In the derivation used, the fibers are assumed to be parallel with the isobars of tissue pressure in the wall.

In the real left ventricle, as well as in a cylindic model of the left ventricle the shells change shape during deformation and muscle fibers cross isobaric surfaces. The discrepancies between the fibrous shell model and the cylinder model are relatively small. When the relation between fiber stress and cavity volume is known, fiber strain can be derived using the principle of conservation of energy. Simple approximations for the cylindric wall with a geometric coupling between the shells say $\sigma_f/P_{lv} = 1 + 3\,V_{lv}/V_w$, and for natural fiber strain $\Delta e_f = (⅓)\Delta \ln (1 + 3\,V_{lv}/V_w)$. Thus, macroscopic cardiac hemodynamics are related to microscopic myocardial fiber function. In contrast with fiber stress, circumferential stress in the wall of a chamber is strongly dependent on geometry.

Received for publication 29 August 1989 and in final form 31 August 1990.

REFERENCES

Arts, T., and R. S. Reneman. 1987. Conversion of fiber stress to global left ventricular pump work. *In* Activation, Metabolism, and Perfusion of the Heart, S. Sideman, editor. Martinus Nijhoff, Dordrecht, The Netherlands. 353–364.

Arts, T., and R. S. Reneman. 1988. The importance of the geometry of the heart to the pump. *In* Starling's Law of the Heart Revisited, H. ter Keurs and M. Noble, editors. Kluwer Academic Publishers Group, Dordrecht, The Netherlands. 94–111.

Arts, T., and R. S. Reneman. 1989. Dynamics of left ventricular wall and mitral valve mechanics: a model study. *J. Biomech.* 22:261–271.

Arts, T., P. C. Veenstra, and R. S. Reneman. 1979. A model of the mechanics of the left ventricle. *Ann. Biomed. Eng.* 7:299–318.

Arts, T., P. C. Veenstra, and R. S. Reneman. 1982. Epicardial deformation and left ventricular wall mechanics during ejection in the dog. *Am. J. Physiol.* 243:H379–H390.

Beyar, R., and S. Sideman. 1984. A computer study of the left ventricular performance based on fiber structure, sarcomere dynamics, and transmural electrical propagation velocity. *Circ. Res.* 55:358–375.

Chadwick, R. S. 1982. Mechanics of the left ventricle. *Biophys. J.* 39:279–288.

Falsetti, H. L., R. E. Mates, C. Grant, D. G. Greene, and I. L. Bunnell. 1970. Left ventricular wall stress calculated from one plane cineangiography—an approach to force–velocity analysis in man. *Circ. Res.* 26:71–83.

Feigl, E. O., G. A. Simon, and D. L. Fry. 1967. Auxotonic and isometric cardiac force transducers. *J. Appl. Physiol.* 23:597–600.

Huisman, R. M. 1980. Comparison of models used to calculate left ventricular wall force. *Med. & Biol. Eng. & Comput.* 18:133–144.

Huyghe, J. M. R. J. 1986. Non-linear finite element models of the beating left ventricle and the intramyocardial coronary circulation. Ph.D. thesis. Eindhoven University of Technology, The Netherlands.

Janz, R. F. 1982. Estimation of local myocardial stress. *Am. J. Physiol.* 242:H875–H881.

Kim, H. C., B. G. Min, M. M. Lee, J. D. Seo, Y. W. Lee, and M. C. Han. 1985. Estimation of local cardiac wall deformation and

regional wall stress from biplane coronary cineangiograms. *IEEE (Inst. Electr. Electron. Eng.) Trans. Biomed. Eng.* 32:503–511.

Mirsky, I. 1969. Left ventricular stresses in the intact human heart. *Biophys. J.* 9:189–208.

Mirsky, I. 1973. Ventricular and arterial wall stresses based on large deformation analysis. *Biophys. J.* 13:1141–1159.

Pao, Y. C., R. A. Robb, and E. L. Ritman. 1976. Plain-strain finite-element analysis of reconstructed diastolic left ventricular cross-section. *Ann. Biomed. Eng.* 4:232–249.

Perl, A., A. Horowitz, and S. Sideman. 1986. Comprehensive model for the simulation of left ventricle mechanics. Part I: model description and simulation procedure. *Med. & Biol. Eng. & Comp.* 24:145–149.

Puff, V. A. 1960. Die Morphologie des Bewegungsablaüfes der Herzkammern. *Anat. Anz.* 108:342–350.

Regen, D. M. 1984. Myocardial stress equations: fiber stresses of the prolate spheroid. *J. Theor. Biol.* 109:191–215.

Regen, D. M. 1988. Effect of chamber shape and fiber orientation on relations between fiber dynamics and chamber dynamics. *Ann. Biom. Eng.* 16:589–607.

Skalak, R. 1982. Approximate formulas for myocardial fiber stresses. *J. Biomech. Eng.* 104:162–163.

Streeter, D. D., and W. T. Hanna. 1973. Engineering mechanics for successive states in canine left ventricular myocardium. II. Fiber angle and sarcomere length. *Circ. Res.* 33:656–664.

Torrent Guasp, F. 1971. The Cardiac Muscle. Juan March Foundation, Madrid.

Waldman, L., D. Nosan, F. Villarreal, and J. Covel. 1988. Relation between transmural deformation and local myofiber direction in the canine left ventricle. *Circ. Res.* 63:550–562.

Woods, R. H. 1892. A few applications of a physical theorem to membranes in the human body in a state of tension. *J. Anat. Physiol.* 26:362–370.

Yin, F. C. P. 1981. Ventricular wall stress. *Circ. Res.* 49:729–842.